Phase transitions of the ferroelectric math xmlns="http://www.w3.org/1998/Math/MathML">mrow>msub>mrow>mo>(/mo>msub>mi>ND/mi>mn>4/mn>/msub>mo>)/mo>/mrow>mn>2/mn>/msub>msub>mi>FeCl/mi>mn>5/mn>/msub>mo>·/mo>msub>mi mathvariant="normal">D/mi>mn>2/mn>/msub>mi mathvariant="normal">O/mi>/mrow>/math> under magnetic field

Shaozhi Li and Randy S. Fishman

Phys. Rev. B **104**, L060407 — Published 17 August 2021

DOI: 10.1103/PhysRevB.104.L060407

Phase transitions of the ferroelectric $(ND_4)_2FeCl_5 \cdot D_2O$ under a magnetic field

Shaozhi Li[1] and Randy S. Fishman[1]

[1]*Materials Science and Technology Division, Oak Ridge National Laboratory, Oak Ridge, Tennessee 37831, USA*

Due to the strong coupling between magnetism and ferroelectricity, $(ND_4)_2FeCl_5 \cdot D_2O$ exhibits several intriguing magnetic and electric phases. In this Letter, we include higher-order onsite anisotropic spin interactions to explain the ferroelectric phase transitions of $(ND_4)_2FeCl_5 \cdot D_2O$ in a magnetic field and to produce the large weights of high-order harmonic components in the cycloid structure that are observed from neutron diffraction experiments. Moreover, we predict a new ferroelectric phase sandwiched between the FE II and FE III phases in a magnetic field. By emphasizing the importance of the higher-order spin anisotropic interactions, our work provides a framework to understand multiferroic materials with rich phase diagrams.

Introduction. — The interplay between charge, lattice, and spin degrees of freedoms induces many fascinating phenomena in materials, including multiferroic behavior [1–4], colossal magnetoresistance [5, 6] and stripe order in the cuprates [7, 8] and nickelates [9, 10]. In the past few years, significant progress has been made in understanding and discovering multiferroics [11–13], motivated by the promise of new technological applications in energy transformation and signal generation and processing. In general, there are two types of multiferroic materials: type I, where the ferroelectricity is independent of the magnetic order [14], and type II, which is more interesting because the electric polarization appears as a consequence of the magnetic order[11, 15–20].

Recently, a new type II material $(NH_4)_2FeCl_5 \cdot H_2O$ with a rich phase diagram was discovered [21–23]. In zero field, $(NH_4)_2FeCl_5 \cdot H_2O$ has an incommensurate cycloidal magnetic order in the ac plane with wave vector $\mathbf{Q} = (0, 0, 0.23)$ r.l.u. below 6.9 K [21, 24]. An incommensurate sinusoidal collinear state appears between 6.9 K and 7.5 K [21]. Ferroelectricity below 6.9 K is attributed to the inverse Dzyaloshinskii-Moriya (DM) mechanism, which predicts that the electric polarization is proportional to $(\mathbf{S}_i \times \mathbf{S}_j) \times \mathbf{Q}$, leading to an electric polarization along the a-axis [24]. These properties have been extensively discussed in previous inelastic neutron scattering (INS) experiments [25] and theoretical studies based on density functional theory (DFT) [26] and spin models [27].

An exciting feature of $(NH_4)_2FeCl_5 \cdot H_2O$ is that the direction of the electric polarization can be tuned by a magnetic field [23]. When the magnetic field is applied along the a-axis at low temperature, phase transitions from ferroelectric I (FE I) to ferroelectric II (FE II) to ferroelectric III (FE III) phases are observed. Neutron diffraction measurements show that the magnetic wave vector $\mathbf{Q} = (0, 0, \xi)$ r.l.u. ($\xi = 0.23$ at $H = 0$) smoothly increases with the magnetic field in FE I, jumps to $\mathbf{Q} = (0, 0, 0.25)$ r.l.u. in FE II, and then to $\mathbf{Q} = (0, 0, 0)$ r.l.u. in FE III [28] (see Fig. 1). The critical magnetic fields for these two transitions are about 2.8 T and 4.7 T near zero temperature, respectively. In FE I and FE II, the electric polarization lies along the a-axis; in FE III, the electric polarization rotates to the c-axis. It has been proposed that the microscopic mechanism of multiferroicity changes from the inverse DM interaction in FE I and FE II to p-d hybridization in FE III. While these phase transitions are also observed when the magnetic field is applied along the c-axis, the critical fields become 1.3 T and 2.2 T. The different critical magnetic fields along a- and c-axes imply that the spin interactions are not isotropic in the ac plane.

Current knowledge of the spin structure in $(NH_4)_2FeCl_5 \cdot H_2O$ is limited to zero field. To understand the spin behavior of $(NH_4)_2FeCl_5 \cdot H_2O$ under a magnetic field, we need to carefully consider the effect of spin anisotropy. Previous theoretical investigations use a simplified form for the anisotropy that cannot explain several features of this material, including (a) the strong third $(0, 0, 3\xi)$ and fifth $(0, 0, 5\xi)$ harmonics of the FE I cycloidal state at zero field, (b) the nature of the FE II phase with $\xi = 0.25$, and (c) the different critical fields for the FE II and FE III phases along a and c. In this Letter, we show that all these features can be explained by introducing both second-order (K_2S^2) and fourth-order (K_4S^4) terms to the anisotropy energy. Our results imply that higher-order anisotropic spin interactions are crucial to explain the spin properties of $(ND_4)_2FeCl_5 \cdot D_2O$ and, perhaps, the magnetic phases in other type II multiferroics.

Magnetic Anisotropy. — In general, the magnetic anisotropy in solids is induced by the spin-orbit coupling [29–31], which is given by $H' = \lambda \mathbf{S} \cdot \mathbf{L} - \mu_B \mathbf{S} \cdot \mathbf{H} - 2\mu_B \mathbf{L} \cdot \mathbf{H}$. Here, λ is the spin-orbit coupling strength, $\mathbf{S}$ and $\mathbf{L}$ represent the spin and angular momentum operators, and $\mathbf{H}$ is the magnetic field. Integrating over the angular momentum operator in the atomic limit, the second-order perturbative energy is $E^{(2)} \propto -\lambda^2 \Lambda_{\alpha\beta} S_\alpha S_\beta + 2\mu_B(\delta_{\alpha\beta} - \Lambda_{\alpha\beta}) S_\alpha H_\beta$, where α and β are indexes for x, y, and z. By considering crystal symmetry, $\lambda^2 \Lambda_{\alpha\beta} S_\alpha S_\beta$ can be reduced to $K_2 S_z^2$ in $SrFeO_2$ [16], $Sr_3Fe_2O_5$ [32], $TbMnO_3$ [16], and Ag_2MnO_2 [33]. The term $2\mu_B(\delta_{\alpha\beta} - \Lambda_{\alpha\beta} S_\alpha H_\beta)$ induces anisotropic g-factors. If the spin-orbit coupling λ is strong, the fourth-order

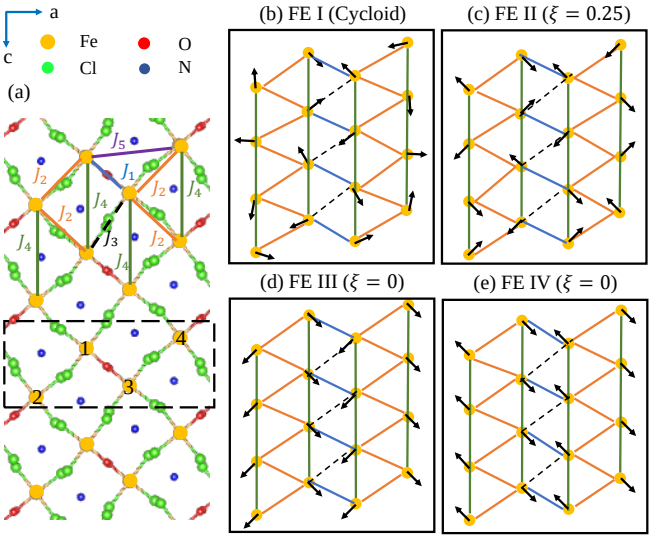

FIG. 1: Crystal structure and magnetic order. (a) Crystal structure of $(ND_4)_2FeCl_5 \cdot D_2O$ in the ac plane. Five different exchange interactions are labeled with different colors. The dashed-rectangle represents one unit cell with four Fe atoms labeled by Arabic numbers. (b) - (e) Spin configurations for four different FE phases.

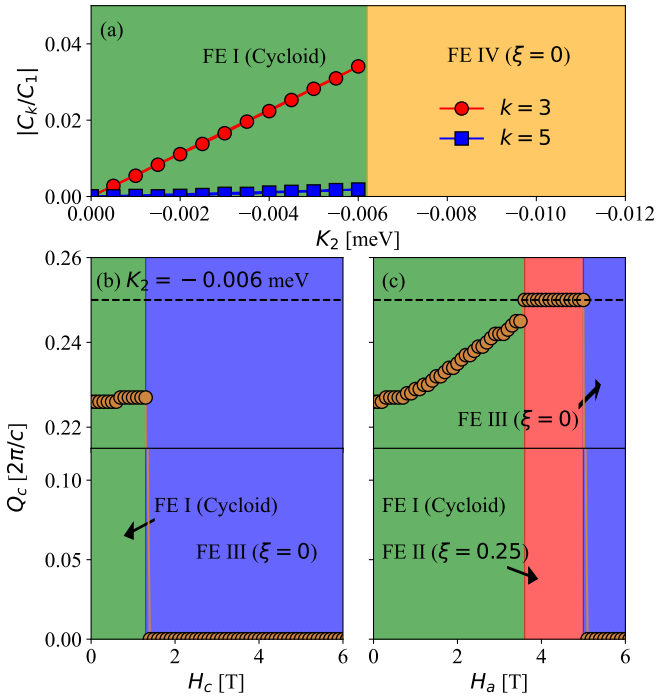

FIG. 2: Phase diagrams at $K_4 = 0$. Panel(a) plots $|\frac{C_3}{C_1}|$ and $|\frac{C_5}{C_1}|$ as a function of K_2. Panels (b) and (c) plot the evolution of the wave vector Q_c as a function of the magnetic fields H_c and H_a, respectively.

perturbative energy $E^{(4)} \propto -\lambda^4 U_{\alpha\beta\gamma\eta} S_\alpha S_\beta S_\gamma S_\eta$ must also be considered.

In this letter, we study the effect of the onsite anisotropic interaction $K_2 S_a^2 + K_4 S_a^4$ in $(ND_4)_2FeCl_5 \cdot D_2O$, where $K_2 S_a^2$ and $K_4 S_a^4$ originate from the second-order and fourth-order perturbative terms. The full spin Hamiltonian for $(ND_4)_2FeCl_5 \cdot D_2O$ is given by

$$H = \sum_{i,j} J_{i,j} \boldsymbol{S}_i \cdot \boldsymbol{S}_j + D \sum_i (S_{i,b})^2 + K_2 \sum_i (S_{i,a})^2 + K_4 \sum_i (S_{i,a})^4 + g\mu_B \sum_i (H_a S_{i,a} + H_c S_{i,c}), \quad (1)$$

where $\boldsymbol{S}_i$ is the spin operator of the Fe^{3+} ion on site i with length $S = 5/2$ and $J_{i,j}$ is the exchange interaction, which is labeled in Fig. 1(a). D, K_2, and K_4 are the single ion anisotropic interactions. If not stated otherwise, we use previous INS studies [25] to set $\{J_1, J_2, J_3, J_4, J_5\} = \{0.178, 0.0641, 0.0289, 0.0566, 0.0447\}$ meV and $D = 0.0183$ meV. Notice that the early spin model only included the easy-plane anisotropy $D > 0$, which makes the spins lie in the ac plane, while ignoring the anisotropy of the spins within the ac plane [26].

We use a variational technique [34] to solve for the spin state by minimizing the energy as a function of variational parameters such as the wavevector (discussed in the supplementary material [35]). Three trial wave functions are used to obtain four different magnetically ordered states, which are labeled as FE I, FE II, FE III, and FE IV (see Fig. 1). The magnetic wave vector is labeled as $\mathbf{Q} = (0, 0, \xi)$ r.l.u.. FE I refers to the cycloidal state with $\xi < 0.25$; FE II and FE IV are antiferromagnetic states with $\xi = 0.25$ and $\xi = 0$, respectively; FE III has spins that are canted by the magnetic field with $\xi = 0$. While both FE III and FE IV have $\xi = 0$, FE III and FE IV are distinct states that appear at high and intermediate to low fields, respectively.

The second-order anisotropy.— We begin with the second-order interaction K_2 and set the fourth-order coefficient K_4 to zero. Figure. 2(a) shows the phase transition from FE I to FE IV as K_2 increases. The critical value for the phase transition is about $K_2 = -0.0061$ meV. A polarized neutron diffraction experiment showed that the reflection intensities at $(0, 0, 3\xi)$ and $(0, 0, 5\xi)$ are about $I_3/I_1 = 0.0076$ and $I_5/I_1 = 0.0038$, implying that the cycloidal structure of $(ND_4)_2FeCl_5 \cdot D_2O$ is distorted [21]. In our variational approach, the ratio $\frac{I_k}{I_1}$ is given by $|\frac{C_k}{C_1}|^2$ because we assume that the a component of the spin at site $\mathbf{r}$ equals $S_a(\mathbf{r}) = \sum_{k>0} C_k \cos(-k\mathbf{Q}\mathbf{r} + \theta_k)$, where k is an integer, and $\mathbf{Q} = (0, 0, \xi)$. When $k = 1$, the spin state is an undistorted cycloid. Both spin anisotropy and a magnetic field distort the cycloid, producing higher-order harmonics. When only second-order anisotropy is considered, the maximum predicted values of $|C_3/C_1|$ (I_3/I_1) and $|C_5/C_1|$ (I_5/I_1) in FE I are about 0.038 (0.0014) and 0.0015 (2.25×10^{-6}), much smaller than the experimental results.

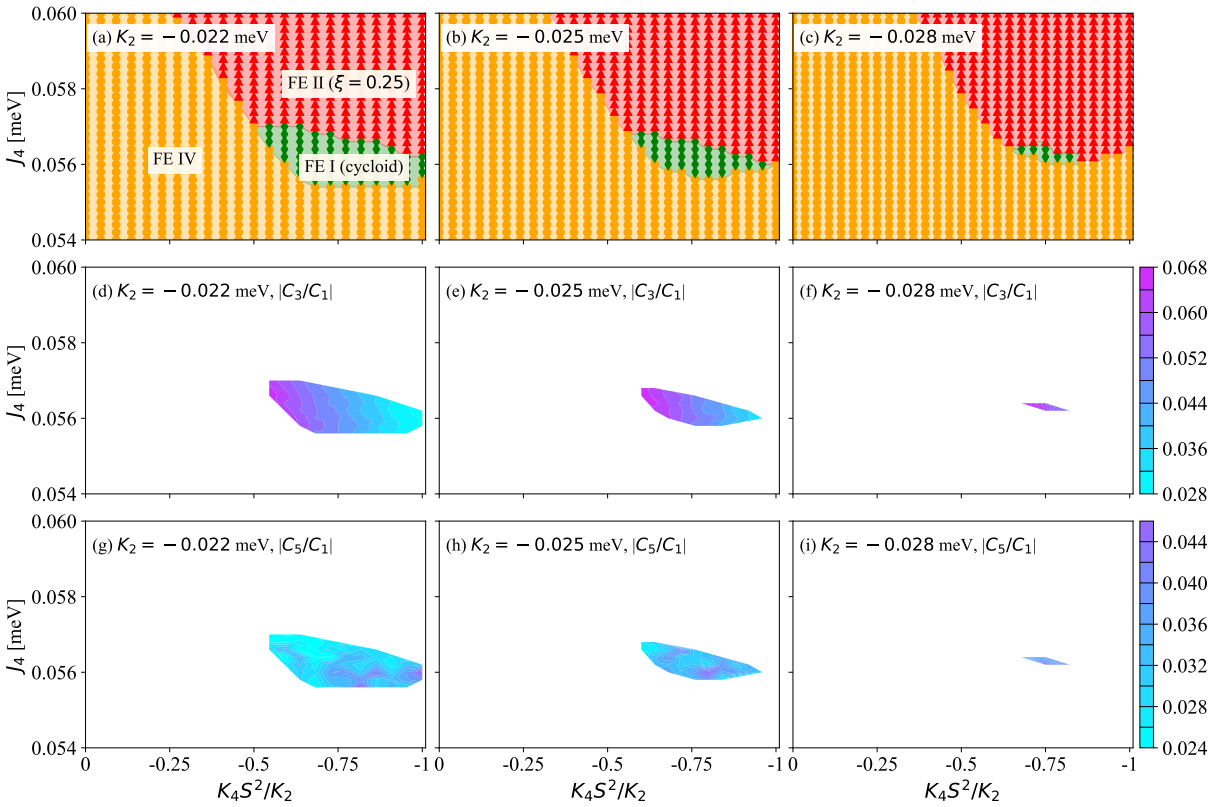

FIG. 3: Phase diagrams for $K_2 = -0.22$, -0.025, and -0.028 meV. (a) - (c) Phase diagrams in the plane of J_4 and K_4S^2/K_2 for three different K_2 values. (d) - (f) $|C_3/C_1|$ in the cycloidal state for three different K_2 values. (g) - (i) $|C_5/C_1|$ in the cycloidal state for three different K_2 values.

We now study the evolution of the spin structures under a magnetic field with $K_2 = -0.006$ meV, which produces a relative large third harmonic $|C_3/C_1|$ in the cycloidal state. Figures 2 (b) and 2 (c) plot the change of the wave vector $Q_c = \xi\frac{2\pi}{c}$ with the magnetic fields H_c and H_a, respectively, where c is the lattice constant along the c-axis. When a field along c (H_c) is applied, FE I directly transforms into FE III. When a field along a (H_a) is applied, FE II appears between FE I and FE III. In the cycloidal state, the wave vector Q_c weakly depends on H_c, but it smoothly increases with H_a.

These theoretical results are inconsistent with the experimental results in two respects. First, the third and fifth harmonics are weak compared to the experimental values. Second, FE II is missing when the magnetic field is applied along the c-axis. These inconsistencies can be addressed by adding the fourth-order anisotropy.

The fourth-order anisotropy. — To understand the fourth-order anisotropy, we calculate the phase diagrams in the $\{J_4, K_4S^2\}$ plane for three different values of K_2 in Fig. 3. In Figs. 3(a)- 3(c), solid symbols represent simulation results and phase boundaries lie at the middle of two data points. These plots show that FE II is located on the right upper side and FE IV is located on the left bottom side. The cycloidal phase FE I resides between FE II and FE IV. As $|K_2|$ increases, the FE IV region grows toward the right upper side and the FE I region shrinks. FE I disappears when $K_2 < -0.028$ meV. Figures 3(d)-3(f) and Figures 3(g)- 3(i) show the weight of the third ($|C_3/C_1|$) and fifth harmonic ($|C_3/C_1|$) components in the cycloidal state, respectively. $|C_3/C_1|$ smoothly decreases as $|K_4|$ increases, while there is no monotonic behavior for $|C_5/C_1|$. The maximal value of $|C_3/C_1|$ is about 0.06 located at the left upper corner in Figs. 3(d)-3(f), and $|C_5/C_1| \sim 0.03$ in that parameter region shown in Figs. 3(g)- 3(i). While these values are still smaller than the experimental values, they are much larger than the results at $K_4 = 0$, especially with $|C_5/C_1|$ enhanced by a factor of ten. It has been proposed that the strong spin-lattice interaction in $(ND_4)_2FeCl_5 \cdot D_2O$ [21] induces nonuniform spin-spin interactions that could further enhance the weight of the third and fifth harmonics. It would be interesting to study the effect of the spin-lattice interaction in $(ND_4)_2FeCl_5 \cdot D_2O$, but such a study is beyond our current focus.

Next, we study the phase transitions under a magnetic field. To be consistent with the microscopic model proposed in Ref. [25], we set $J_4 = 0.0566\,\text{meV}$. The value $K_2 = -0.075\,\text{meV}$ is used because it can produce relative large $|C_3/C_1|$ and $|C_5/C_1|$ in a wide region of K_4

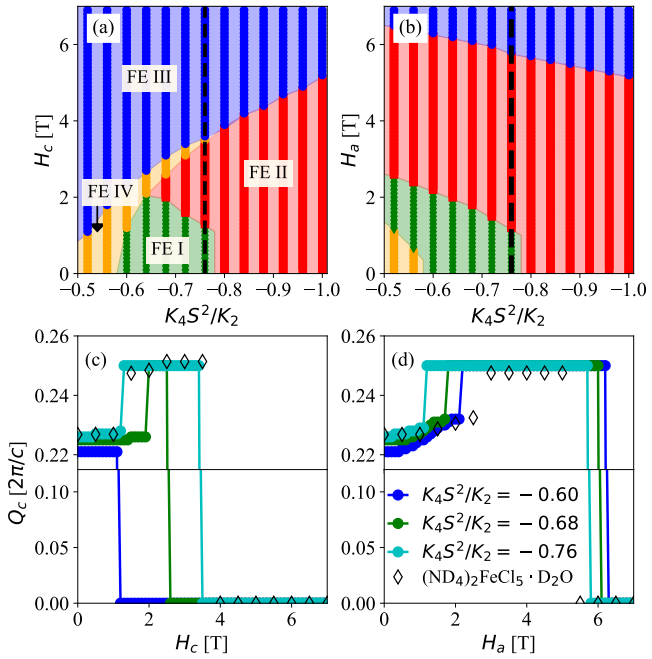

FIG. 4: Phase transitions under the magnetic field at $J_4 = 0.0566$ meV and $K_2 = -0.025$ meV. Panels (a) and (b) plot the phase diagram in the H_c and K_4 plane and in the H_a and K_4 plane, respectively. Panels (c) and (d) plot the change of the magnetic wave vector Q_c as a function of H_c and H_a, respectively. Diamond symbols represent experimental results obtained from Ref. [28].

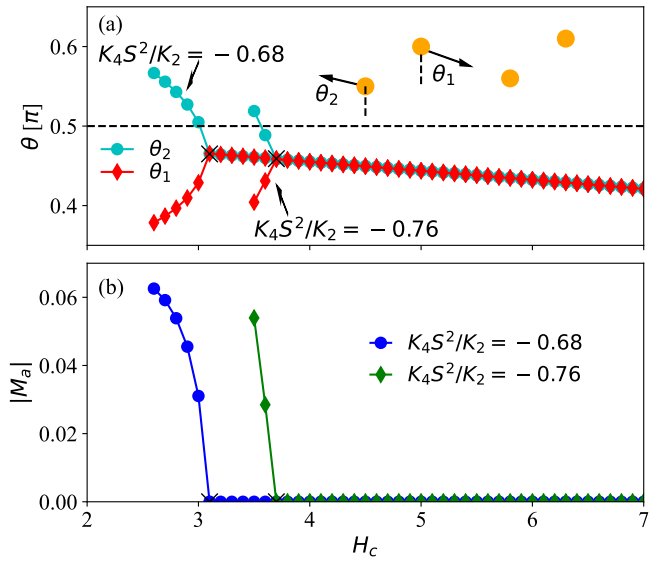

FIG. 5: Comparisons of FE III and FE IV. Panel (a) plots spin angles of two neighboring sites along the c-axis. Panel (b) plots the a component of the uniform magnetization M_a. Crossing symbols represent the phase boundary between FE III and FE IV. Here, J_2 and K_2 have the same values as those in Fig. 4.

at $J_4 = 0.0566$ meV, as shown in Fig. 3(e). While a slightly different value of K_2 can quantitatively change results, the qualitative results remain the same. Figures 4(a) and 4(b) show the phase diagram in the H_c and K_4S^2/K_2 plane and the H_a and K_4S^2/K_2 plane, respectively. Compared to Figs. 2(b) and 2(c), the phase diagram is richer when the fourth-order anisotropy is included.

At zero magnetic field, the magnetic ground state is FE IV for $K_4S^2/K_2 > -0.58$, FE I for $-0.58 > K_4S^2/K_2 > -0.78$, and FE II for $-0.78 > K_4S^2/K_2 > -1$. When a field is applied along c, both FE IV and FE II directly transform into FE III at high fields. For the FE I state, there are two different sets of phase transitions. When $-0.58 > K_4S^2/K_2 > -0.65$, FE I transforms to FE IV and then to FE III as H_c increases; for $-0.58 > K_4S^2/K_2 > -0.65$, FE I first transforms to FE II, then to FE IV, and finally to FE III.

The change of the magnetic wave vector Q_c is different for these two sets of phase transitions. Figure 4(c) plots the evolution of Q_c under H_c for three different values of K_4S^2/K_2. For $K_4S^2/K_2 = -0.6$ (the former set of phase transitions), Q_c is independent of H_c in FE I, and jumps to zero in FE IV. For $K_4S^2/K_2 = -0.68$ and $K_4S^2/K_2 = -0.76$ (the latter set of phase transitions), Q_c weakly depends on H_c in FE I and then jumps to 0.25 $\frac{2\pi}{c}$ in FE II. Finally, Q_c is zero in FE IV and FE III. The change of Q_c for the latter phase transitions is consistent with the results of the neutron diffraction measurements [28], which are labeled as the diamond symbols in Figs. 4(c) and 4(d) .

Interestingly, the phase transition under H_a is very different from that under H_c. Rather than transform directly into FE III, FE IV transforms continuously from FE I to FE II and then to FE III as H_a increases. Compared to the case with field along c, FE IV is absent when $-0.58 > K_4S^2/K_2 > -0.78$. We also find that the critical value of H_a for FE III is much larger than that of H_c. The critical value of H_a for the phase transition from FE I to FE II is close to the value of H_c when $-0.64 > K_4S^2/K_2 > -0.78$. We plot the change of Q_c with field H_a in Fig. 4(d). Here, the increase of Q_c in FE I is more prominent than that in Fig. 4(c) for the field along c.

In $(ND_4)_2FeCl_5 \cdot D_2O$, FE II and FE III appear near $H_c = 1.5$ T and $H_c = 4$ T or $H_a = 2.7$ T and $H_a = 5$ T, respectively [28]. In our simulations, the critical values of H_c (H_a) for these two states are 1.3 T (1.2 T) and 3.5 T (5.8 T) at $K_4S^2/K_2 = -0.076$ and $K_2 = -0.025$ meV [see the dashed line in Figs. 4(a) and 4(b)]. The small discrepancy between our theoretical and experimental results could originate from the change of exchange and anisotropy interactions in $(ND_4)_2FeCl_5 \cdot D_2O$ in a magnetic field [25].

Since both FE IV and FE III have zero wave vector, they cannot be distinguished based on measurements of

Q_c. Here, we propose a different method to distinguish FE IV and FE III experimentally. We label the spin angles of neighbouring sites along the c-axis as θ_1 and θ_2, respectively, as shown in Fig. 5(a). While θ_1 and θ_2 are the same for FE III, they are different for FE IV. Figure 5(a) plots these two angles versus the field H_c at $K_4S^2/K_2 = -0.68$ and $K_4S^2/K_2 = -0.76$ using $J_4 = 0.0566$ meV and $K_2 = -0.025$ meV. Notice that θ_1 increases and θ_2 decreases as H_c increases in FE IV and that they are equal in FE III. FE IV transforms into FE III when $\theta_1 = \theta_2$. We set the phase boundary between FE III and FE IV at a data point where $\theta_2 = \theta_1$ and label it as a crossing symbol in Fig. 5. Figure 5(b) shows the a component of the magnetization $|M_a|$. Under H_c, the c component of the magnetization for both FE III and FE IV are nonzero. However, M_a is zero for FE III and it has a finite value for FE IV. As FE IV transforms into FE III, $|M_a|$ rapidly vanishes. Hence, FE III and FE IV can be experimentally distinguished by examining the behavior of $|M_a|$ under field H_c.

In a magnetic field, the phase transition from FE II to FE IV is first order, while the transition from FE IV to FE III is second order because θ_1 and θ_2 continuously change near the phase boundary. If as proposed, the electric polarization $\boldsymbol{P}$ in FE III is induced by p-d orbital hybridization [28], then $\boldsymbol{P} \propto \sum_i (\boldsymbol{S}\cdot\boldsymbol{r}_i)^2 \boldsymbol{r}_i$ would lie along the c-axis ($\boldsymbol{r}_i$ represents the vector from the Fe atom to its nearest Cl atom or D_2O). If the d-p orbital hybridization mechanism also holds in FE IV, then $\boldsymbol{P}$ would rotate away from the c-axis to the a-axis with a small angle ($< 0.01\pi$), causing a small a component to coexist with a large c component of the polarization [36]. Interestingly, this coexistence is observed in $(NH_4)_2FeCl_5 \cdot H_2O$ near $H_c = 4$ T [23].

Discussion and Conclusions. — We have studied the spin model proposed for $(ND_4)_2FeCl_5 \cdot D_2O$ and examined the phase transitions under a magnetic field. We find that the second-order onsite spin anisotropy alone cannot describe the magnetic behavior of $(ND_4)_2FeCl_5 \cdot D_2O$, including the weights of the third and fifth harmonic components of the cycloidal state and the appearance of the FE II state under a magnetic field along c-axis. With the fourth-order onsite spin anisotropy, the weights of the third and fifth harmonic components are enhanced and all the observed magnetic states of $(ND_4)_2FeCl_5 \cdot D_2O$ are obtained in our simulations. Moreover, we predict a new FE IV state in the magnetic phase diagram. This state can be identified by measuring the uniform magnetization perpendicular to the magnetic field. The existence of the nonzero uniform magnetization perpendicular to the magnetic field is due to the spin anisotropy. Our results imply that the higher-order onsite spin anisotropy is essential to explain the magnetic properties of $(ND_4)_2FeCl_5 \cdot D_2O$.

Our results qualitatively describe phase transitions of $(ND_4)_2FeCl_5 \cdot D_2O$ under a magnetic field. To quantitatively describe the magnetic behavior, it would be necessary to carefully consider all parameters in the spin model, including the change of the exchange interactions under a magnetic field, to fine tune K_2 and K_4, and to include the spin-lattice interaction proposed in Ref. [28].

It is well known that the chemical substitution can change the spin anisotropy in solids and induce different magnetic ground states [37]. It would be interesting to study the effect of doping in $(ND_4)_2FeCl_5 \cdot D_2O$, including the magnetic phase transitions with possible appearance of the FE IV phase, and dynamical spin excitations. Our theoretical work on higher-order anisotropic interactions provides a guideline to understand the effect of doping both in $(ND_4)_2FeCl_5 \cdot D_2O$ and other type-II multiferroics.

We would like to acknowledge useful conversations with Xiaojian Bai, Minseong Lee, Jan Musfeldt, and Wei Tian. This work was supported by the U.S. Department of Energy, Office of Basic Energy Sciences, Materials Sciences and Engineering Division. This research used resources of the Compute and Data Environment for Science (CADES) at the Oak Ridge National Laboratory, which is supported by the Office of Science of the U.S. Department of Energy under Contract No. DE-AC05-00OR22725.

[1] N. A. Hill, J. Phys. Chem. B **104**, 6694 (2000), URL https://doi.org/10.1021/jp000114x.

[2] Y. Tokura, S. Seki, and N. Nagaosa, Reports on Progress in Physics **77**, 076501 (2014), URL https://doi.org/10.1088/0034-4885/77/7/076501.

[3] N. A. Spaldin and R. Ramesh, Nature Materials **18**, 203 (2019), URL https://doi.org/10.1038/s41563-018-0275-2.

[4] Y. Wang, J. Hu, Y. Lin, and C.-W. Nan, NPG Asia Materials **2**, 61 (2010), URL https://doi.org/10.1038/asiamat.2010.32.

[5] Z. Qiu, D. Hou, J. Barker, K. Yamamoto, O. Gomonay, and E. Saitoh, Nature Materials **17**, 577 (2018), URL https://doi.org/10.1038/s41563-018-0087-4.

[6] M. Baldini, T. Muramatsu, M. Sherafati, H.-k. Mao, L. Malavasi, P. Postorino, S. Satpathy, and V. V. Struzhkin, Proceedings of the National Academy of Sciences **112**, 10869 (2015).

[7] Y. Zhang, C. Lane, J. W. Furness, B. Barbiellini, J. P. Perdew, R. S. Markiewicz, A. Bansil, and J. Sun, Proceedings of the National Academy of Sciences **117**, 68 (2020), ISSN 0027-8424, https://www.pnas.org/content/117/1/68.full.pdf, URL https://www.pnas.org/content/117/1/68.

[8] H. Zhao, Z. Ren, B. Rachmilowitz, J. Schneeloch, R. Zhong, G. Gu, Z. Wang, and I. Zeljkovic, Nature Materials **18**, 103 (2019), URL https://doi.org/10.1038/s41563-018-0243-x.

[9] J. Zhang, D. M. Pajerowski, A. S. Botana, H. Zheng, L. Harriger, J. Rodriguez-Rivera, J. P. C. Ruff, N. J. Schreiber, B. Wang, Y.-S. Chen, et al., Phys. Rev. Lett.

122, 247201 (2019), URL https://link.aps.org/doi/10.1103/PhysRevLett.122.247201.

[10] A. M. Merritt, A. D. Christianson, A. Banerjee, G. D. Gu, A. S. Mishchenko, and D. Reznik, Scientific Reports **10**, 11426 (2020), URL https://doi.org/10.1038/s41598-020-67963-x.

[11] D. Khomskii, Physics **2**, 20 (2009), URL https://physics.aps.org/articles/v2/20.

[12] S. Dong, J.-M. Liu, S.-W. Cheong, and Z. Ren, Advances in Physics **64**, 519 (2015), URL https://doi.org/10.1080/00018732.2015.1114338.

[13] M. Fiebig, T. Lottermoser, D. Meier, and M. Trassin, Nature Reviews Materials **1**, 16046 (2016), URL https://doi.org/10.1038/natrevmats.2016.46.

[14] J. Wang, J. B. Neaton, H. Zheng, V. Nagarajan, S. B. Ogale, B. Liu, D. Viehland, V. Vaithyanathan, D. G. Schlom, U. V. Waghmare, et al., Science **299**, 1719 (2003), ISSN 0036-8075, URL https://science.sciencemag.org/content/299/5613/1719.

[15] T. Kimura, T. Goto, H. Shintani, K. Ishizaka, T. Arima, and Y. Tokura, Nature **426**, 55 (2003), URL https://doi.org/10.1038/nature02018.

[16] H. J. Xiang, S.-H. Wei, M.-H. Whangbo, and J. L. F. Da Silva, Phys. Rev. Lett. **101**, 037209 (2008), URL https://link.aps.org/doi/10.1103/PhysRevLett.101.037209.

[17] A. Malashevich and D. Vanderbilt, Phys. Rev. Lett. **101**, 037210 (2008), URL https://link.aps.org/doi/10.1103/PhysRevLett.101.037210.

[18] M. Kenzelmann, A. B. Harris, S. Jonas, C. Broholm, J. Schefer, S. B. Kim, C. L. Zhang, S.-W. Cheong, O. P. Vajk, and J. W. Lynn, Phys. Rev. Lett. **95**, 087206 (2005), URL https://link.aps.org/doi/10.1103/PhysRevLett.95.087206.

[19] I. V. Solovyev, Phys. Rev. B **83**, 054404 (2011), URL https://link.aps.org/doi/10.1103/PhysRevB.83.054404.

[20] I. A. Sergienko and E. Dagotto, Phys. Rev. B **73**, 094434 (2006), URL https://link.aps.org/doi/10.1103/PhysRevB.73.094434.

[21] W. Tian, H. Cao, J. Wang, F. Ye, M. Matsuda, J.-Q. Yan, Y. Liu, V. O. Garlea, H. K. Agrawal, B. C. Chakoumakos, et al., Phys. Rev. B **94**, 214405 (2016), URL https://link.aps.org/doi/10.1103/PhysRevB.94.214405.

[22] W. Tian, H. B. Cao, A. J. Clune, K. D. Hughey, T. Hong, J.-Q. Yan, H. K. Agrawal, J. Singleton, B. C. Sales, R. S. Fishman, et al., Phys. Rev. B **98**, 054407 (2018), URL https://link.aps.org/doi/10.1103/PhysRevB.98.054407.

[23] M. Ackermann, D. Brning, T. Lorenz, P. Becker, and L. Bohatý, New Journal of Physics **15**, 123001 (2013), URL https://doi.org/10.1088/1367-2630/15/12/123001.

[24] J. A. Rodríguez-Velamazán, Ó. Fabelo, Á. Millán, J. Campo, R. D. Johnson, and L. Chapon, Scientific Reports **5**, 14475 (2015), URL https://doi.org/10.1038/srep14475.

[25] X. Bai, R. S. Fishman, G. Sala, D. M. Pajerowski, G. Garlea, T. Hong, M. Lee, J. A. Fernandez-Baca, H. Cao, and W. Tian, arXiv:2008.06827 (2020), URL https://arxiv.org/abs/2008.06827.

[26] A. J. Clune, J. Nam, M. Lee, K. D. Hughey, W. Tian, J. A. Fernandez-Baca, R. S. Fishman, J. Singleton, J. H. Lee, and J. L. Musfeldt, npj Quantum Materials **4**, 44 (2019), URL https://doi.org/10.1038/s41535-019-0180-1.

[27] L. Minseong, arXiv: 2103.08500 (2021), URL https://arxiv.org/abs/2103.08500.

[28] J. A. Rodríguez-Velamazán, O. Fabelo, J. Campo, A. Millán, J. Rodríguez-Carvajal, and L. C. Chapon, Phys. Rev. B **95**, 174439 (2017), URL https://link.aps.org/doi/10.1103/PhysRevB.95.174439.

[29] J. Liu, H.-J. Koo, H. Xiang, R. K. Kremer, and M.-H. Whangbo, The Journal of Chemical Physics **141**, 124113 (2014), URL https://doi.org/10.1063/1.4896148.

[30] D. Dai, H. Xiang, and M.-H. Whangbo, Journal of Computational Chemistry **29**, 2187 (2008), URL https://onlinelibrary.wiley.com/doi/abs/10.1002/jcc.21011.

[31] S. Li, Phys. Rev. B **103**, 104421 (2021), URL https://link.aps.org/doi/10.1103/PhysRevB.103.104421.

[32] H.-J. Koo, H. Xiang, C. Lee, and M.-H. Whangbo, Inorg. Chem. **48**, 9051 (2009), URL https://doi.org/10.1021/ic9007526.

[33] S. Ji, E. J. Kan, M.-H. Whangbo, J.-H. Kim, Y. Qiu, M. Matsuda, H. Yoshida, Z. Hiroi, M. A. Green, T. Ziman, et al., Phys. Rev. B **81**, 094421 (2010), URL https://link.aps.org/doi/10.1103/PhysRevB.81.094421.

[34] R. S. Fishman, Phys. Rev. B **88**, 104419 (2013), URL https://link.aps.org/doi/10.1103/PhysRevB.88.104419.

[35] See Supplemental Material at XXXXXX for the details of the variational method.

[36] H. Murakawa, Y. Onose, S. Miyahara, N. Furukawa, and Y. Tokura, Phys. Rev. B **85**, 174106 (2012), URL https://link.aps.org/doi/10.1103/PhysRevB.85.174106.

[37] J. Wang, R. S. Fishman, Y. Qiu, J. A. Fernandez-Baca, G. Ehlers, K.-C. Liang, Y. Wang, B. Lorenz, C. W. Chu, and F. Ye, Phys. Rev. B **98**, 214425 (2018), URL https://link.aps.org/doi/10.1103/PhysRevB.98.214425.